LA-UR-20-20313
Approved for public release; distribution is unlimited.

Title: Beyond the Arrhenius rate law in simulating the shock-driven decomposition of polyimide

Author(s): Peterson, Jeffrey Hammett
Coe, Joshua Damon

Intended for: Report

Issued: 2020-01-13

Beyond the Arrhenius rate law in simulating the shock-driven decomposition of polyimide

Jeffrey H. Peterson, XCP-2
Joshua D. Coe, T-1

January 10, 2020

Abstract

Building off of previous work simulating the shock-driven decomposition of polysulfone[1], we present simulations of the shock-driven decomposition of polyimide. In agreement with the previous work, we find that the Arrhenius rate equation is insufficient for quantitatively reproducing the experimental wave profiles, and we also find that the Arrhenius rate equation cannot reproduce many of the qualitative features of the wave. In light of these results, we examined both an empirical Eyring rate equation as well as the Shock Reactive Flux Method (SRFM) as presented by Valone [2] and found neither to be able to fully capture the quantitative behavior of the measured wave. More specifically, we found that the Eyring equation was only marginally better than an Arrhenius rate law in achieving the very fast reaction rates required to reproduce data at high particle velocities. While the SRFM offered two additional parameters for fitting reaction behavior, we found that the rate law was only able to reproduce the data over a limited range of particle velocities while not being able to reproduce measured shock velocities.

1 Introduction

When subjected to shock loading, many polymers and organic materials undergo spontaneous decomposition resulting in a multi-wave structure that can be observed through a number of different diagnostics [3–8]. Evidence for this reaction can also be seen in the Hugoniot loci where a break occurs around 20 GPa that corresponds to the transition from reactants to products [9]. Previously, we had attempted to model the decomposition of one such polymer, polysulfone (PSF), by linking two equations of state for reactants and products through a rate law in the hydrodynamics simulation code `xRAGE` [1]. While we were able to achieve qualitative agreement between the simulation results and both legacy data and more modern velocimetry data, we were unable to quantitatively reproduce either the shape of the wave itself or the effect of the reaction on the shock velocity. We determined that we were limited by the Arrhenius

rate law that is only a function of the temperature of the system which meant that it was not sensitive enough to changing conditions at the shock front.

More specifically, we noted that the Arrhenius rate law seemed to only be valid over a very small range of parameter space and so it could not be used to describe the more general behavior of the reacting polymer over a range of impact velocities. We also observed that while the simulation was able to qualitatively reproduce the wave behavior for shock transmission experiments that were probed using laser velocimetry, the agreement was much worse for the embedded gauge experiments. In those cases, the gauge data showed only subtle effects of the reaction while our simulations predicted a very pronounced two-wave structure. From these observations we came to the conclusion that a new rate law was needed in order to match the behavior over a larger parameter range.

In modeling polyimide (PI), we chose to explore two additional rate laws while also re-examining the Arrhenius rate law. For the first rate law, we chose to use an empirical Eyring-like rate law where the pre-exponential frequency factor in the Arrhenius equation is now a linear function of temperature. The second was derived by Valone [2] based upon the treatment by Tannor and Kohen [10] that we're calling the Shock Reactive Flux Method (SRFM) rate law. Both rate laws were chosen in an effort to broaden the range of reaction rates available for low and high particle velocities, but while the Eyring rate equation is still wholly dependent on temperature, the SRFM rate equation introduces a dependence on the particle velocity.

In this work we examine the effectiveness of each of these rate laws in reproducing three different types of data: 1) historical particle and shock velocity data compiled by Carter and Marsh [9], 2) transmission experiments where laser velocimetry is used to measure the velocity at the interface between the reacting polyimide and a lithium floride (LiF) window, and 3) embedded gauge experiments where the particle velocity within the reacting material is measured directly. We still find that all rate equations have a limited range of applicability for a given set of parameters, but we also find that the SRFM rate equation offers additional flexibility that may be helpful in certain situations.

2 Rate models

The equations of state (EOS) for PI and its reaction products [11] are linked in the `xRAGE` code through a reaction rate law that is coupled to the hydrodynamic state of the material. The reaction progress variable, λ, is calculated by solving the differential equation,

$$\mathcal{R} = \frac{\mathrm{d}\lambda}{\mathrm{d}t} = (\lambda - 1)^n k, \tag{1}$$

where $\mathcal{R}$ is the reaction rate, n is the reaction order and k is a reaction rate constant that couples with the state of the simulation.

For an Arrhenius rate law, the reaction rate constant is purely a function of temperature and is given by

$$k(T) = Z \exp\left(-\frac{T_\mathrm{a}}{T}\right), \tag{2}$$

where T is the temperature, Z is the frequency factor, and T_a is the activation temperature which can be related to an activation energy, E_a, and Boltzmann's constant, k_B, by $T_\mathrm{a} = E_\mathrm{a}/k_\mathrm{B}$. Since the Arrhenius rate law is purely a function of temperature, the important coupling between the hydrodynamics and the reaction are the relative temperatures of the reactants and products Hugoniot loci as discussed by Menikoff [12]. In this context, we define an exothermic reaction as one where the temperature of the material will increase as the reaction progresses, and therefore further conversion of reactants to products will increase the temperature and thereby the rate of reaction. While a negative enthalpy change between reactants and products would normally signify an exothermic reaction at ambient conditions, the enthalpy change is only equal to the liberated heat when the pressure is constant. Under shocked conditions however, the pressure varies with the reaction progress so the enthalpy change does not necessarily predict the effect of temperature on the reaction.

As noted in section 1, the reaction rate for the shock-driven decomposition of polysulfone was not sensitive enough to shock strength, resulting in a reaction that was too fast at low compressions and too slow at high compressions. Noting that the Arrhenius equation describes a Boltzmann distribution of particles attempting to thermally cross an energy barrier, Z represents the frequency at which the particles "collide" with the energy barrier. The Eyring equation proposes that this frequency is itself a linear function of temperature such that

$$k(T) = Z^* T \exp\left(\frac{-T\mathrm{a}}{T}\right) \tag{3}$$

where we treat Z^* as an empirical constant much like the Arrhenius equation. However, it should be recognized that Z^* has a value of $\kappa k_\mathrm{B}/h$ derived from statistical mechanics, where h is Plank's constant and κ is a transmission coefficient which describes the probability of a species passing through the transition to the product state.

The final rate law used for simulating the shock decomposition of PI was derived by Valone [2] based off of the Tannor and Kohen treatment of the reactive flux method [10]. Without going into the derivation, the final result in [2] is his equation 11,

$$k = Z \exp\left(-\frac{T_\mathrm{a}}{T}\right)\left(\Lambda \exp\left(-\theta\Lambda\right) + \sqrt{\pi\theta}\ \mathrm{erfc}\left(-\sqrt{\theta\Lambda}\right)\right), \tag{4}$$

which is a modification to the Arrhenius rate to include the effects of friction and the particle velocity. The two new dimensionless parameters, Λ and θ, are

$$\Lambda = \frac{\sqrt{\frac{1}{4}\gamma^2 + 4\pi^2 Z^2} - \frac{1}{2}\gamma}{\sqrt{\frac{1}{4}\gamma^2 + 4\pi^2 Z^2} + \frac{1}{2}\gamma} \tag{5}$$

and

$$\theta = \frac{mu^2}{2k_{\mathrm{B}}T} \tag{6}$$

that themselves are functions of the friction factor, γ, and the effective mass, m. If both m and γ are set to zero, then the multiplying factor in equation 4 goes to 1 and the original Arrhenius rate equation is recovered. In the low-friction limit, γ goes to zero and Λ goes to 1, resulting in the multiplying factor always being greater than or equal to 1, thereby enhancing the reaction rate.

While the velocity u in this equation represents the particle velocity projected along the reaction coordinate, we make the assumption here that the material is isotropic such that a particle velocity in any direction will affect the reaction in the same way. We will revisit this assumption after presentation of the results.

3 Results

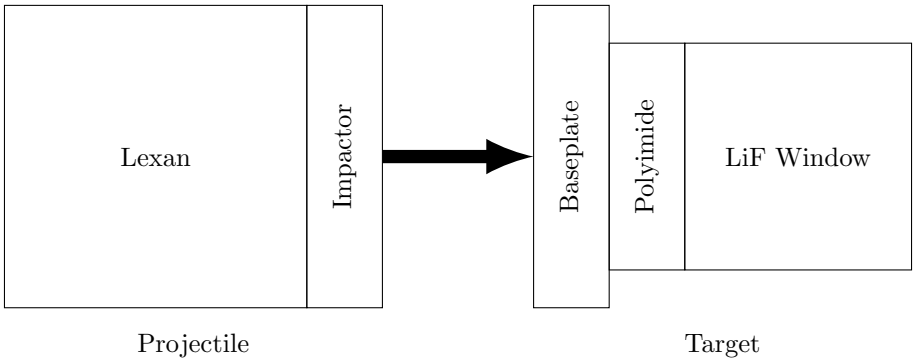

Figure 1: Diagram showing experimental setup for velocimetry data. The shock that results from the projectile striking the target is recorded through PDV or VISAR measurements of the particle velocity at the polyimide-LiF interface.

To evaluate the behavior of these rate laws, four shock experiments [13] were used for comparison with the simulation results, with the setup for each experiment being similar to the transmission experiments described in [1]. In this case, the impactor consisted of either a copper or tantalum plate backed by a polycarbonate projectile fired from the barrel of a two-stage gas gunas shown in figure 1. VISAR and PDV probes were used to measure the velocity on the back side of the PI sample, which is then compared with the velocity measured just inside the window from the simulation. These four experiments were designed to achieve pressures in the polyimide bracketing the transition region. Our results here will focus on the two extremes of these experiments labeled 2s-1104 and 2s-1089 which correspond to shock pressures of approximately 33.3 GPa and 23.7 GPa respectively. The former exhibits an "overdriven" response where the

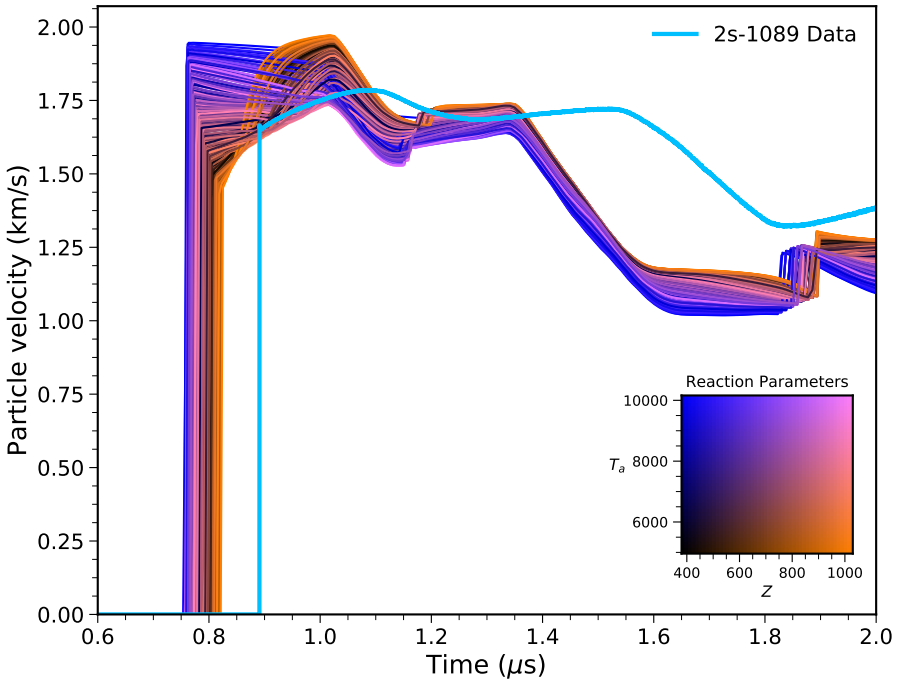

Figure 2: Simulation results for a range of Arrhenius parameters (thin lines) compared to measured velocimetry data (thick blue line). The inset graph shows the color range that corresponds to specific Arrhenius parameters for each simulation that are plotted in the main graph. Shot 2s-1089 corresponds to an input pressure of approximately 23.7 GPa.

reaction timescale is much faster than the hydrodynamics producing a single wave with a rounded profile; the latter is just above the minimum pressure for a reaction and so we observe a two-wave structure.

3.1 Arrhenius Rate Law

In the shock data from figure 2, we can clearly see the two-wave structure as the initial shock, referred to as the $P1$ wave, is immediately followed by a slow rise up to a reacted state known as $P2$. Both the flier and the baseplate are 2.5-mm thick while the PI sample is only 3-mm thick, and as a result rarefaction and additional shock waves have time to form and reach the PI-LiF interface shortly after the reaction wave. More specifically, the rarefaction wave that forms at the aluminum-PI interface can propagate backwards and reflect off of the impactor and reach the LiF window approximately 1.1 μs after the impact, decreasing the particle velocity. Similarly, the second major drop in the plotted data can be attributed to the forward-traveling rarefaction wave that forms at the interface

between the impactor and the polycarbonate projectile behind it.

To fully explore the Arrhenius parameter space, fourteen different values for both Z and T_a were chosen and 196 permutations of the two parameters were simulated using the same setup as the experiment. The frequency factor, Z was varied from 380 to 1030 μs^{-1} while the activation temperature was varied between 4960 and 10160 K both at regular intervals. These results are also plotted alongside the experimental data in figure 2 where the timescales are all adjusted so that $t = 0$ corresponds to the flier impact time[1]. Each parameter combination is identified by a single color that is related to a value for Z and T_a in the inset figure. Faster reactions tend to be more orange in color as Z is larger and T_a is smaller, while slower reactions tend to be more blue where the reverse is true for both parameters. Material behind the shock becomes more dense as the reaction progresses, and this volume change has the effect of doing negative work on the surrounding material. The net effect on the shock itself is therefore to deprive the shock of energy and slow it down. A faster reaction can accomplish this quicker, meaning that the average shock velocity over the transit through PI is overall smaller, a fact reflected in figure 2 by the later arrival times for the orange lines when compared to blue.

We can take a closer look at the these trends by limiting Z to be either very large (orange/pink) or very small (black/blue) as shown in figure 3. Note that while Z spans a range where the maximum value is almost three times the minimum value, the effect of Z on the reaction wave profile is markedly less pronounced than that of T_a which varies by only two times. For example, both the dark black and bright orange lines correspond to $T_a = 4960$ and are reasonably close to each other, while the bright orange and bright pink lines correspond to $Z = 1030$ but display very different behaviors. This behavior is of course due to the fact that T_a exists within the exponential while Z is simply a scaling constant on the rate, making the rate much more sensitive to changes in T_a.

Assuming that the shock arrival time is a good indicator of the overall reaction rate, we can pick two lines that have similar shock arrival times in order to identify how T_a and Z separately influence the reaction wave profile. For example, the dark black line that represents $T_a = 4960$ and $Z = 380$ has a shock arrival time that closely resembles an orange line corresponding to $T_a = 6160$ and $Z = 1030$. Immediately after the shock has arrived, the rate is fairly slow and the reaction is in what can be called the induction regime [12] where heat release from the reaction itself has yet to have significant impact on the rate. At this point, the reaction rate for the simulation with the larger Z value is actually smaller due to the higher activation temperature and so the particle velocity for the orange simulation begins increasing at a slower rate than for the black simulation. Eventually however, the temperature increases enough to where the higher frequency factor results in a larger reaction rate and the orange line overtakes the black line.

[1]For a comparison where the time origin for the data is shifted to better correspond with the simulations see appendix A.

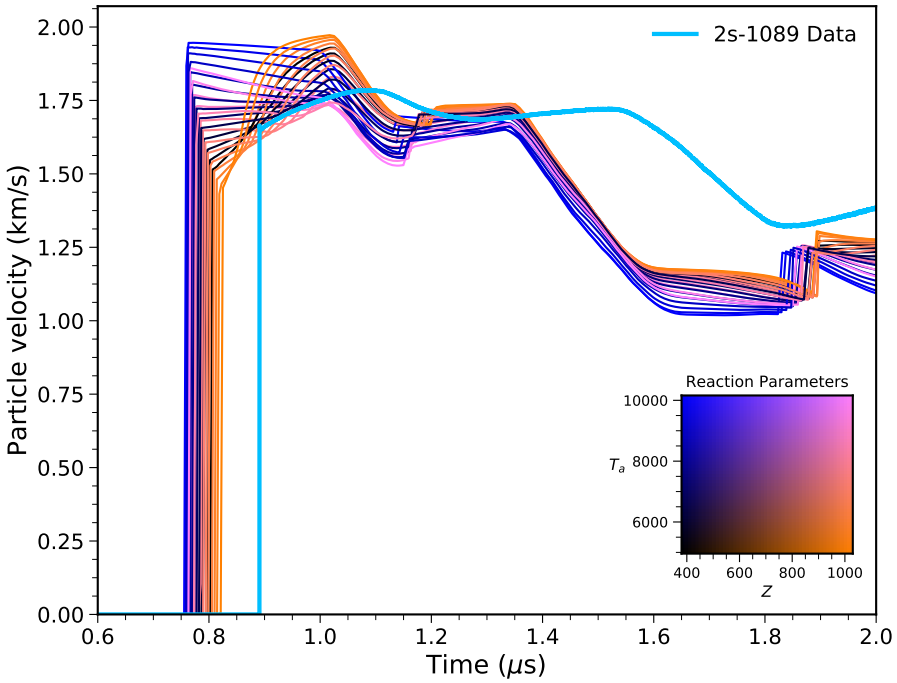

Figure 3: Simulation results for a range of T_a with $Z = 380$ (blue to black) and $Z = 1030$ (pink to orange) compared to measured velocimetry data represented by the thick blue line. Once again, the data inset describes the parameter values in the same way as in figure 2

In our work on polysulfone [1] and for some of the parameters shown here for polyimide (pink and blue regime), the particle velocity of the Lagrangian point actually decreases after the initial shock. We believe this is due to the same negative work being done on the surrounding material by the reaction, which tends to decelerate the area ahead of the reacting zone. Eventually however, the energy released by the reaction raises both the temperature and the pressure, this time doing positive work on the surrounding material and accelerating the particle velocity. Within the induction regime, the effect of the reaction on the wave profile is mainly driven by the intrinsic change in volume due to the reaction while in the thermal runaway regime the behavior is dominated by the volume change caused by the temperature increase.

The same comparison can be made to the higher-pressure shot, 2s-1104, and is shown in figure 4. Once again, we are only showing the range of values for the activation temperature at two different values for Z. The trends are similar to those identified for the simulations of shot 2s-1089, but in this case we observe that at very high reaction rates we begin to better approximate the experimental results. We also are able to observe noticeable differences between

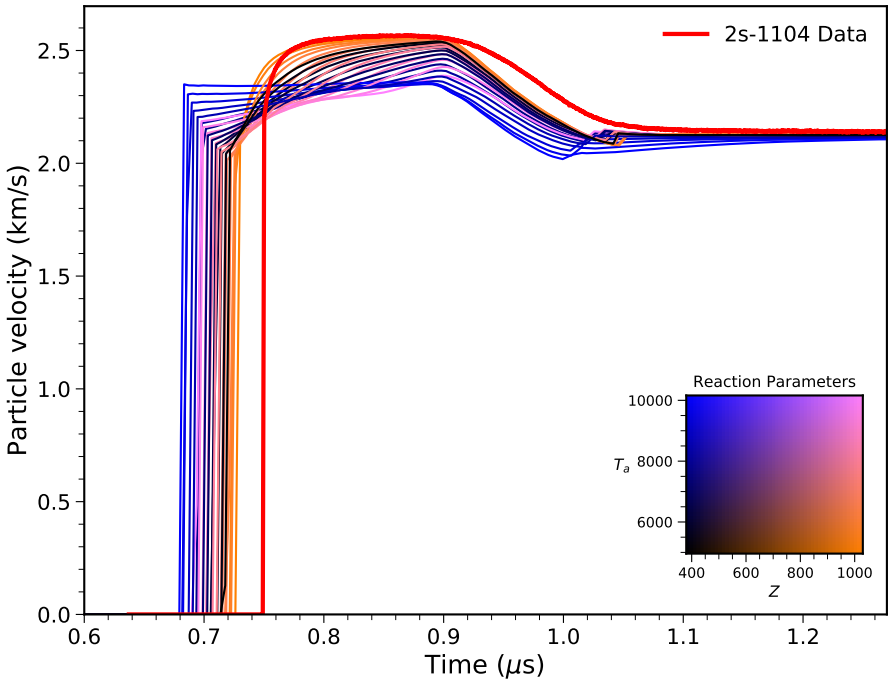

Figure 4: Simulation results for a range of T_{a} with $Z = 380$ (blue to black) and $Z = 1030$ (pink to orange) compared to measured velocimetry data represented by the thick red line. In this case, the experimental results correspond to an input pressure of 33.3 GPa.

the hydrodynamics of the simulation and the experiment. While the simulated wave profile shows a sharp drop due to the reflected rarefaction wave and a small shock around 1 μs, these features aren't seen in the velocimetry data, suggesting that perhaps there is more dissipation, either through the reaction or otherwise, in the real system than is taken into account in the simulation.

3.2 Eyring Rate Law

A key limitation of the Arrhenius rate law is that the parameters required to achieve this agreement in the over-driven regime are not applicable to particle velocities outside of a narrow range; in other words, the Arrhenius rate law is not sensitive enough to different flier velocities. We implemented the Eyring rate law as a possible method for improving this sensitivity and some selected results are presented in Figure 5, where again we are examining the effect of varying the activation temperature but this time with two different values for Z^*. Because `xRAGE` uses temperature units in terms of electron volts instead of Kelvin, the values for Z^* range from 2940 to 7945 $\mu\mathrm{s}^{-1}$-eV^{-1} with figure 5

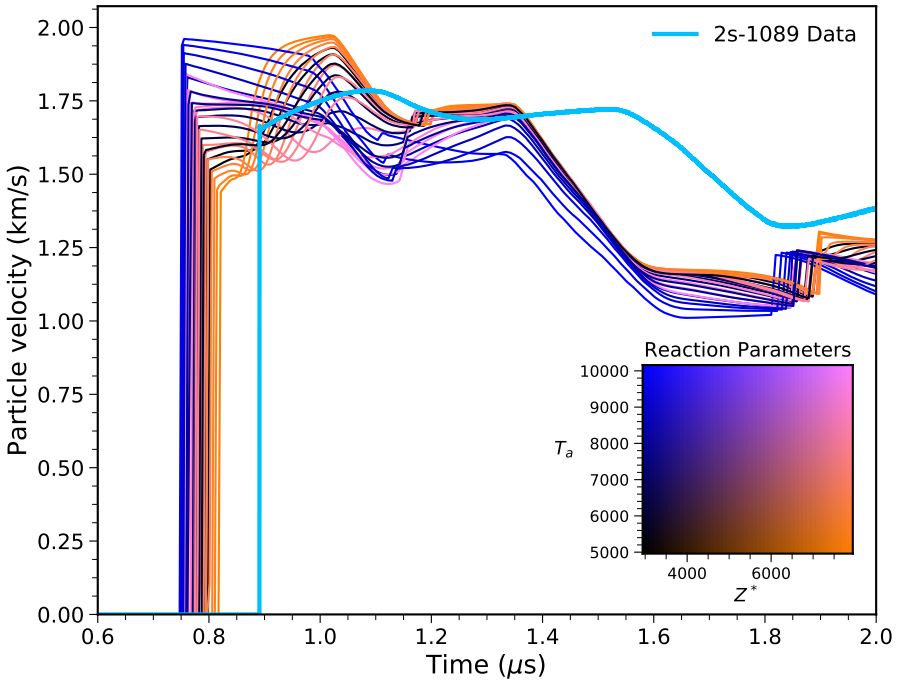

Figure 5: Simulation results of the Eyring rate equation for $Z^* = 2940$ and $Z^* = 7945$ across the same range of activation temperatures as in previous figures compared with shot 2s-1089.

showing the extremes of Z^*. At first glance, Figure 5 closely resembles figure 3, especially in the arrival time of the shock. There is however a key difference in the shape of the wave profile at the beginning of the reaction where the Eyring results show a more significant induction region where the particle velocity is either decreasing or relatively stagnant. The values for Z^* were chosen such that $Z^*T \approx Z$ when $T = 1500$ K, so at the beginning of the reaction the Eyring rate is slower than the Arrhenius rate as the temperature is below 1500 K. As the reaction progresses, the material heats and we observe behavior very similar to that seen with the Arrhenius rate equation. However, we note that the velocimetry data does not imply slow kinetics during the induction phase of the reaction, and instead it shows a steady rise to the $P2$ state beginning immediately after the shock arrives.

Our first observation of the Eyring rate law is that it does not afford much more additional sensitivity than what the Arrhenius rate equation already displayed. This is further reinforced by examining the higher-pressure 2s-1104 shot which is shown in figure 6. We do observe slightly better agreement with the velocimetry data, but we still observe that the shock arrival time at the window is significantly earlier than in the experiment. Furthermore, the kinetic

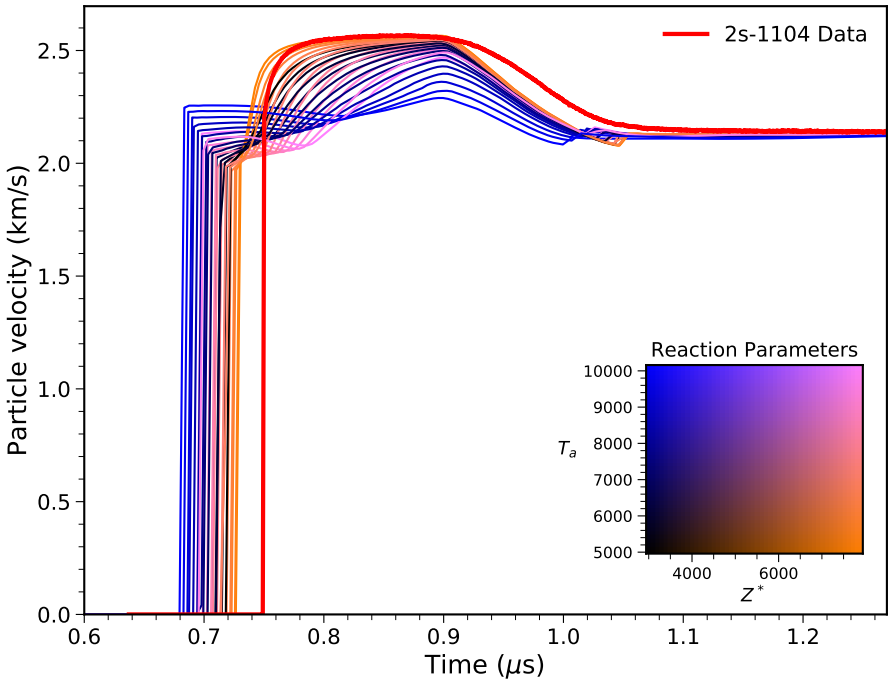

Figure 6: Simulation results of the Eyring rate equation for $Z^* = 2940$ and $Z^* = 7945$ across the same range of activation temperatures as in previous figures compared with shot 2s-1104.

parameters appropriate for the high-pressure impact will still not agree with the lower-pressure experimental data, so we conclude that temperature-dependence alone is not suitable for constructing a rate equation that fully describes the range of wave behaviors for decomposing soft materials.

Furthermore, these experiments show the state of $P1$ state of material that has been reshocked by the window. With a different window materials, we would expect a different wave response both from the hydrodynamics and from the reaction itself. The Eyring rate equation shows that the rate law's pure temperature dependence would likely be insufficient to reproduce differences that would result from different window materials.

3.3 Shock Reactive Flux Method

At this point we have established that temperature dependence alone is insufficient for giving the reaction rate law the needed sensitivity to reproduce the qualitative features of the velocimetry data over a range of impact velocities. One of the defining features of a shock wave is the large kinetic energy of the moving material, and in the case of chemical reactions the magnitude of this

kinetic energy can often be comparable to the barrier described by transition state theory. In this sense, we seek a rate law that takes into account the fact that the bulk velocity due to the shock will bias the movement of the reacting particle population along the reaction coordinate.

One such rate law has been proposed by Valone [2] that we presented in equation 4 and includes a multiplier on the standard Arrhenius rate law. The dependence of the rate law on both the effective mass parameter as well as the particle velocity and temperature is contained within the parameter

$$\theta = \frac{mu^2}{2k_{\mathrm{B}}T} \tag{7}$$

that will vary depending on how hard the material is shocked.

For illustration, we can think about the case of when the reacting materials are ideal gasses in order to better understand this dimensionless parameter. Equation 7 can be rewritten by first recognizing that the internal energy is related to the particle velocity through

$$E - E_0 = \frac{1}{2}(u_{\mathrm{p}} - u_0)^2, \tag{8}$$

which comes from the Rankine-Hugoniot jump conditions. If we assume that $u_0 = 0$ and that the material has a constant heat capacity, we can re-write this equation in terms of temperature,

$$\widetilde{C}_V(T_{\mathrm{s}} - T_0) = \frac{1}{2}u_{\mathrm{p}}^2, \tag{9}$$

where subscript 's' denotes that this is the shocked temperature. Solving for T_{s} and remembering that the hypothetical material is an ideal gas, i.e. $\widetilde{C}_V = 3k_{\mathrm{B}}/2m$, yields

$$T_{\mathrm{s}} = \frac{m}{3k_{\mathrm{B}}}u_{\mathrm{p}}^2, \tag{10}$$

which can be substituted into equation 7 to give

$$\theta = \frac{1}{6}\frac{T_{\mathrm{s}}}{T}. \tag{11}$$

In our case, the temperature, T, deviates from the shock temperature only due to the reaction so we can re-write this as

$$\theta = \frac{1}{6}\frac{T_{\mathrm{s}}}{T_{\mathrm{s}} + \Delta T_{\mathrm{rxn}}} \tag{12}$$

where ΔT_{rxn} is the temperature change caused by the energy release of the reaction. As a result we can see that as the shock strength increases, this ratio will grow and asymptotically approach a constant value at very high shock temperatures. Indeed, barring any phase changes, we can observe this exact behavior in our calculated equations of state for both the reactants and products. As the reaction energy increases, the rate at which this ratio asymptotes to a

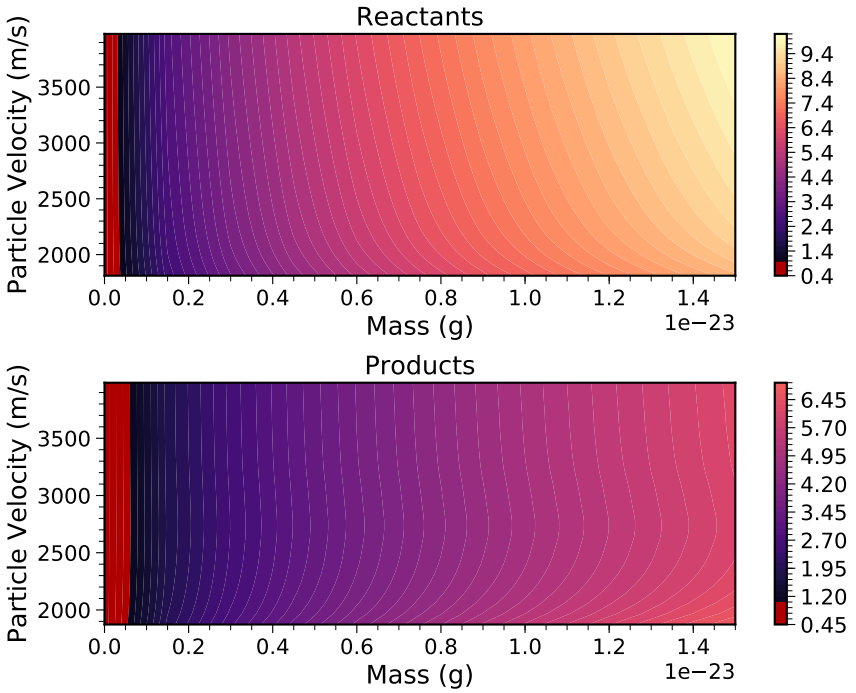

Figure 7: Value of the multiplier term (equation 13) in the SRFM rate equation for the products and reactants as a function of both particle velocity and effective mass when $\gamma = 1900$. The temperature and particle velocities for both products and reactants are taken from the principal Hugoniot loci for both materials in the calculation of θ.

constant is decreased, which basically has the effect of emphasizing the thermal contribution more than the particle velocity in the rate equation.

Additionally, we can analyze the effect of θ on the rate equation by graphing the value of the term that multiplies the underling Arrhenius expression,

$$\Lambda \exp\left(-\theta\Lambda\right) + \sqrt{\pi\theta}\ \mathrm{erfc}\left(-\sqrt{\theta\Lambda}\right), \tag{13}$$

as a function of effective mass and particle velocity. This is shown in figure 7 with values below 1, i.e. those that would decrease the rate, highlighted in dark red for when the friction factor, γ, equals 2700. A similar plot is shown in figure 8 but for $\gamma = 270150$.

From these plots, we see that this term will decrease the rate constant as the reaction progresses from reactants to products since the products are generally at a higher temperature due to the exothermic nature of the reaction. Second, we also see that the rate equation is a very weak function of particle velocity when the effective mass is small (i.e. between 0 and 4.0×10^{-24} for the reactants).

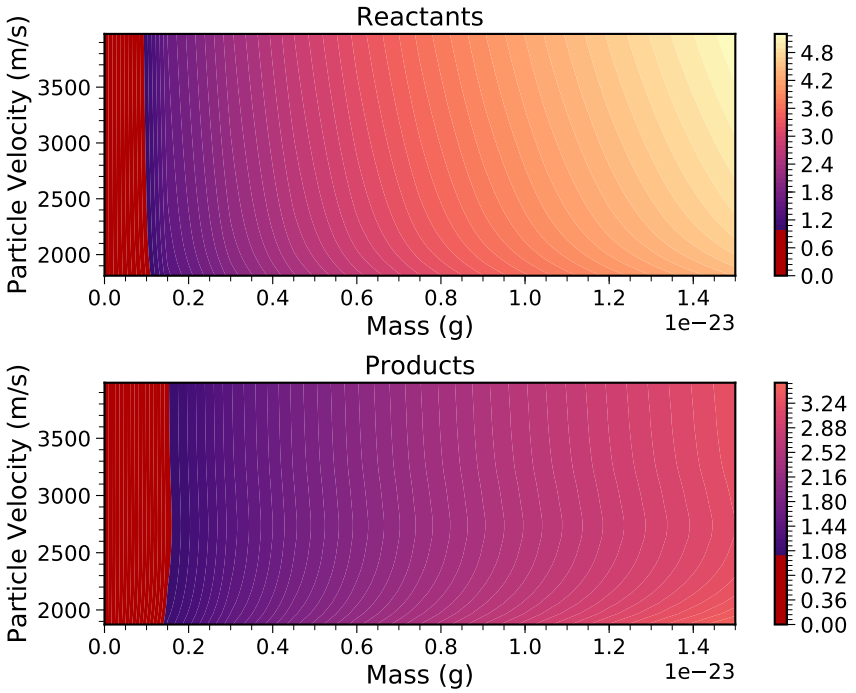

Figure 8: Value of the multiplier term (equation 13) in the SRFM rate equation for the products and reactants as a function of both particle velocity and effective mass when $\gamma = 270150$.

But even at higher effective masses, we see that the multiplier only varies by at most 10% over the range of particle velocities that bracket the transition region. Finally, the dominant effect of γ is really only to scale the final multiplier and has very little effect on the actual sensitivity of the rate equation to the particle velocity.

Eleven different values for the effective mass ranging from 0 to 1.5×10^{-23} along with another eleven values for γ logarithmically spaced from zero to 270150 were selected in order to provide a wide range of behaviors for the rate equation. These parameters were paired with Arrhenius parameters of $Z = 430$ and $T_{\mathrm{a}} = 7760$, and because the SRFM rate law reduces to Arrhenius for $\gamma = 0$ and $m = 0$, the original Arrhenius behavior can be approximated by the $m = 0$ case in the plots. Each permutation of the SRFM parameters was simulated and compared to the experimental results with those for $\gamma = 1900$ shown in figure 9 for shot 2s-1089 and in figure 10 for shot 2s-1104.

Immediately we see that the behavior is similar to that already observed with the Arrhenius and Eyring rate equations. However, we do see that certain combinations of parameters yield rise times and shapes that are more similar to what is observed in the velocimetry data. We also see multiple inflections in the

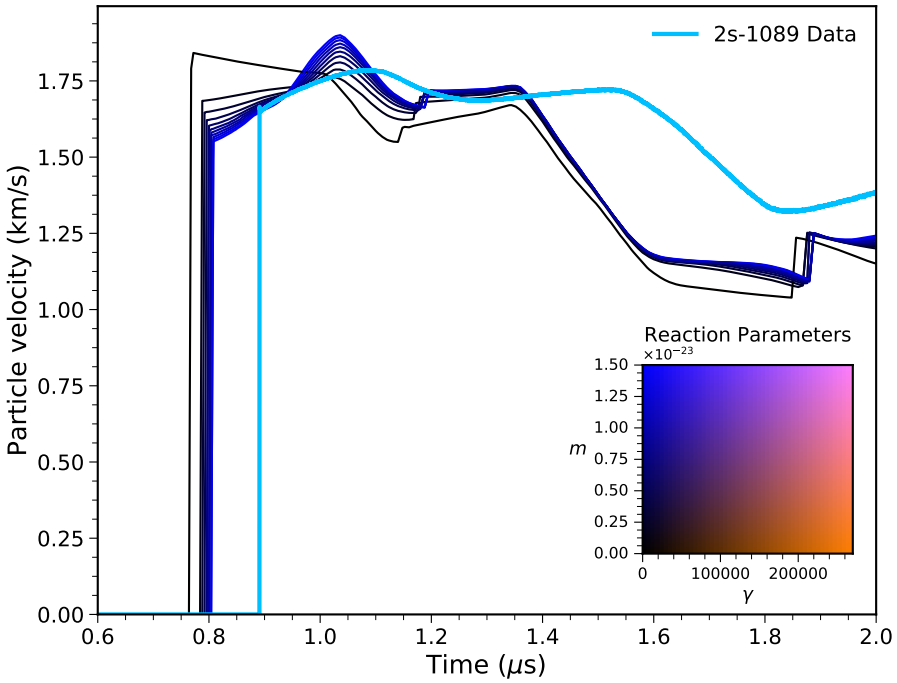

Figure 9: Simulation results using the SRFM rate equation when $\gamma = 1900$ for various values for the effective mass, m, being compared to shot 2s-1089. The Arrhenius parameters for these simulations are $Z = 430$ and $T_a = 7760$.

simulated wave profiles that result from the competing effects of temperature increasing the reaction rate through the Arrhenius term and decreasing the rate through the multiplying term from equation 13. Examining the comparison to shot 2s-1104 in figure 10, we see that the increased sensitivity to the particle velocity has contributed to a wave profile that more closely matches the velocimetry data, but we still see that the reaction is too fast for shot 2s-1089 and too slow for shot 2s-1104. Furthermore, we see that the shock arrival time is still much sooner than is observed in the experiments, perhaps suggesting that a one-step reaction may be insufficient for capturing the full range of behaviors for polyimide over a wide range of impact velocities.

4 Summary, discussion, and future directions

Results for the simulation of polyimide over a wide range of kinetic parameters have been shown for an Arrhenius rate equation, an Eyring rate equation, and the shock reactive flux method rate equation derived by Valone [2]. In agreement with previous results for polysulfone [1], we find that the Arrhenius rate equation

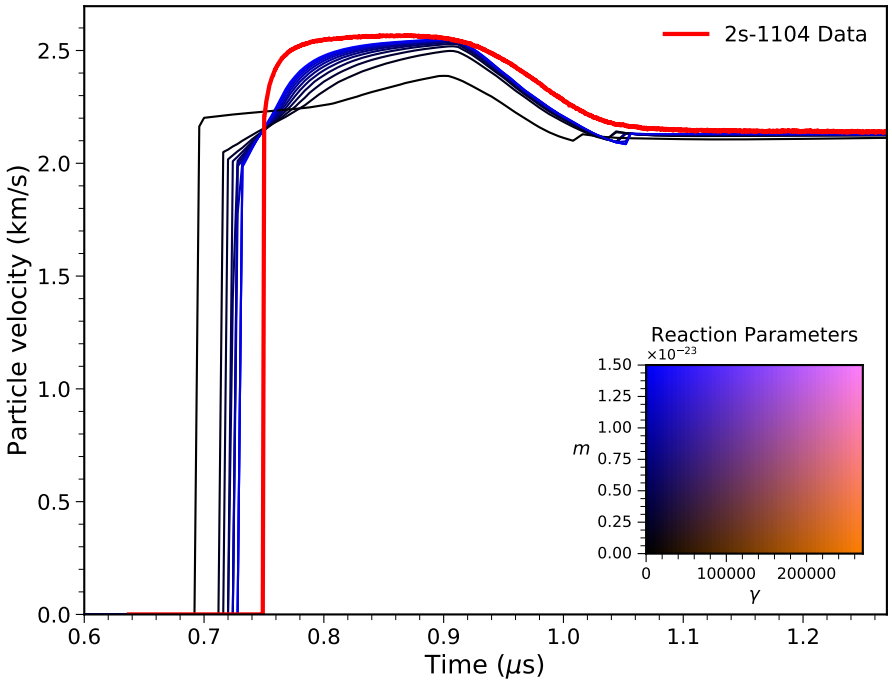

Figure 10: Simulation results using the SRFM rate equation when $\gamma = 1900$ for various values for the effective mass, m, being compared to shot 2s-1104. The Arrhenius parameters for these simulations are $Z = 430$ and $T_a = 7760$.

is insufficient for reproducing the sensitivity of the reaction rate to changes in impact velocity for flier experiments. Similarly, the Eyring rate equation did not introduce significantly higher sensitivity to warrant its use for these applications.

The results from the SRFM rate equation are more encouraging though as they demonstrate that significantly more sensitivity can be introduced through a proper rate equation. Based off of the trends identified so far, it is conceivable that an even higher effective mass could further enhance the sensitivity of the rate to the particle velocity, but the central issue with this rate law is that the particle velocity is not always an appropriate indicator for the driving force behind the reaction. For example, we can think about the situation where the end of the PI is a free surface instead of being adjacent to a window. In this case, a rarefaction wave would quickly accelerate the material to approximately twice the original particle velocity. However, the temperature and pressure in the rarefaction wave are decreasing and one would expect the reaction not to proceed as quickly even though this equation would likely result in a rate increase. Similarly, we can imagine the situation of the PI being against a material with very high impedance, in which case a strong reflected shock will propagate back through the PI and reduce the particle velocity to near zero but

also increase the reaction rate.

It may be that the compensating effects of the particle velocity and temperature tend to offset each other in the correct way, but this would need to be examined in more detail through further simulations. However, introducing a pressure-dependence instead of a particle-velocity-dependence would side-step this issue and allow for better treatment of both re-shocked conditions as well as rarefactions. We believe that the SRFM rate equation may be appropriate in certain circumstances, but more work is needed in order to fully understand the parameter space.

A Time-shifted data comparisons

For all of the data comparisons presented, the time origin has been set to be the time of impact either by construction in the simulations or as reported in the data. While this choice of $t = 0$ is unambiguous and simple, it confounds the shock arrival time with the uncertainty in the base plate equation of state and the measurement uncertainty for the impact time. In an attempt to alleviate these sources of uncertainty, we adjusted the time origin so that the shock arrival time for shot 2s-1104 corresponds with the median arrival time for the simulations of a given rate model. The time offset required to achieve this was then applied to shot 2s-1089. The following figures are all identical to the above figures with the addition of this time offset to aid comparison.

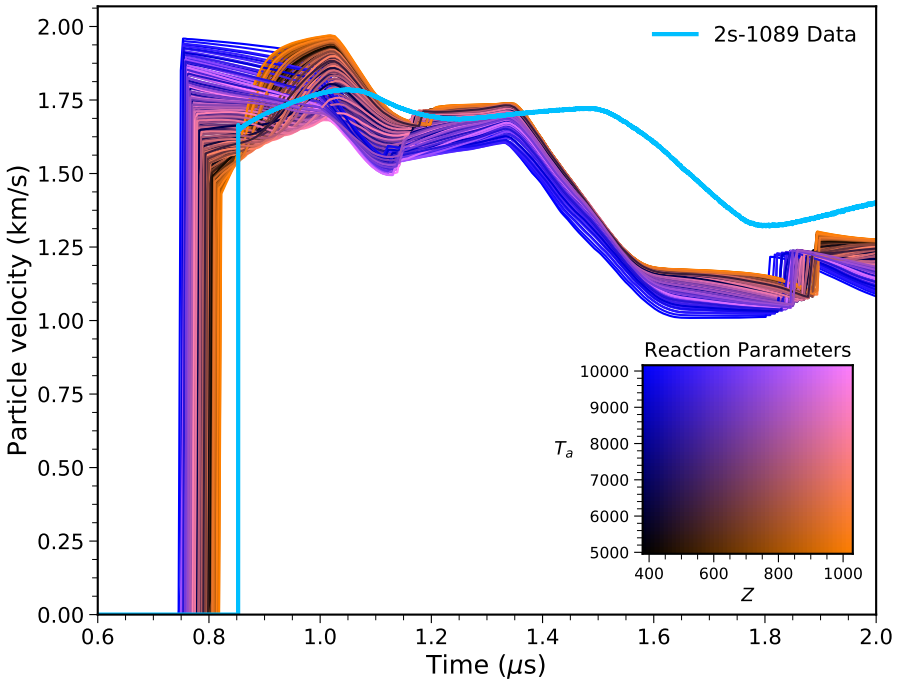

Figure 11: Simulation results for a range of Arrhenius parameters (thin lines) compared to measured velocimetry data (thick blue line). The inset graph shows the color range that corresponds to specific Arrhenius parameters for each simulation that are plotted in the main graph. Shot 2s-1089 corresponds to an input pressure of approximately 23.7 GPa.

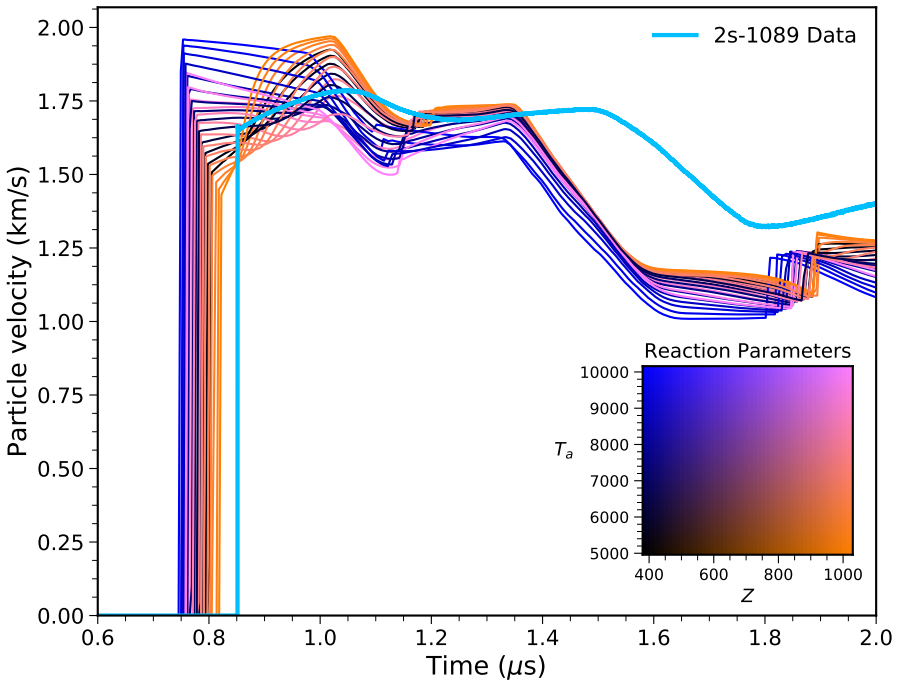

Figure 12: Simulation results for a range of T_a with $Z = 380$ (blue to black) and $Z = 1030$ (pink to orange) compared to measured velocimetry data represented by the thick blue line. Once again, the data inset describes the parameter values in the same way as in figure 2

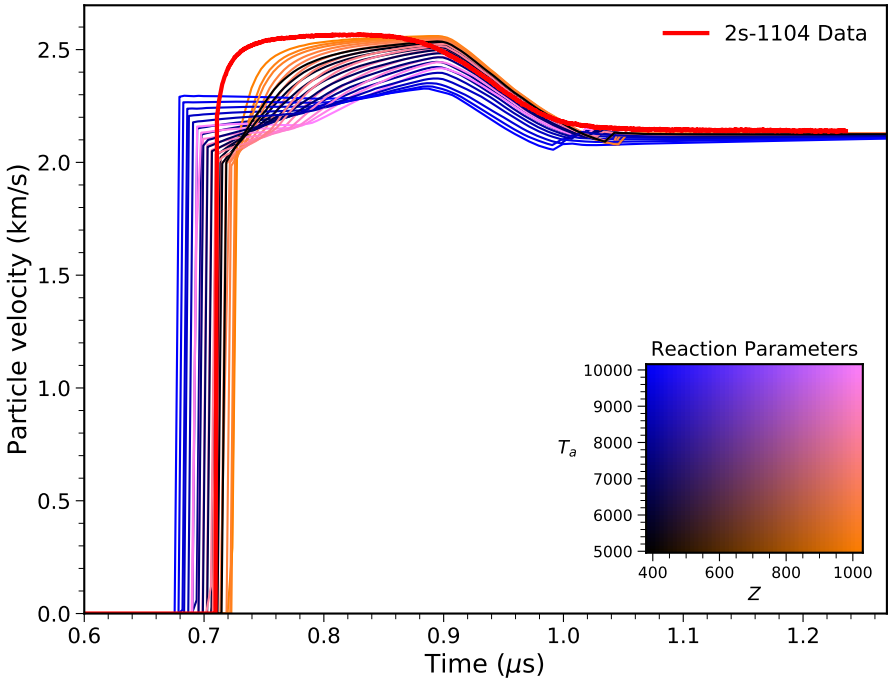

Figure 13: Simulation results for a range of T_{a} with $Z = 380$ (blue to black) and $Z = 1030$ (pink to orange) compared to measured velocimetry data represented by the thick red line. In this case, the experimental results correspond to an input pressure of 33.3 GPa.

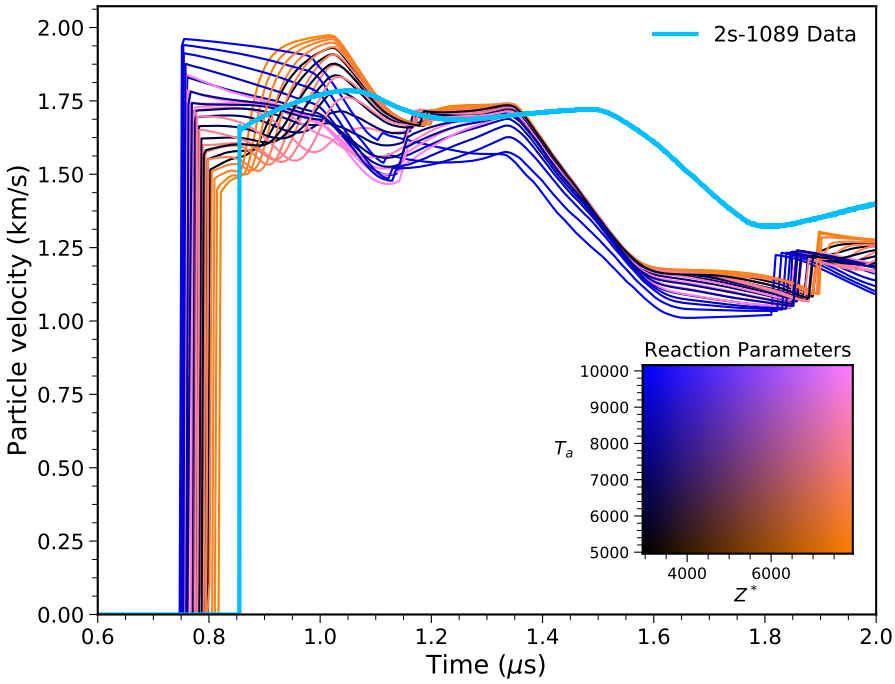

Figure 14: Simulation results of the Eyring rate equation for $Z^* = 2940$ and $Z^* = 7945$ across the same range of activation temperatures as in previous figures compared with shot 2s-1089.

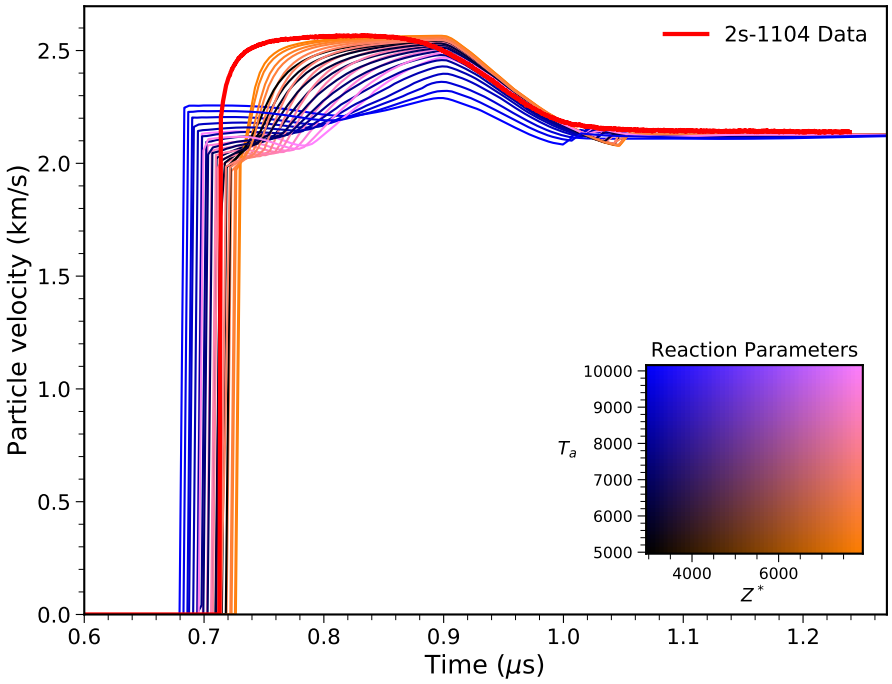

Figure 15: Simulation results of the Eyring rate equation for $Z^* = 2940$ and $Z^* = 7945$ across the same range of activation temperatures as in previous figures compared with shot 2s-1104.

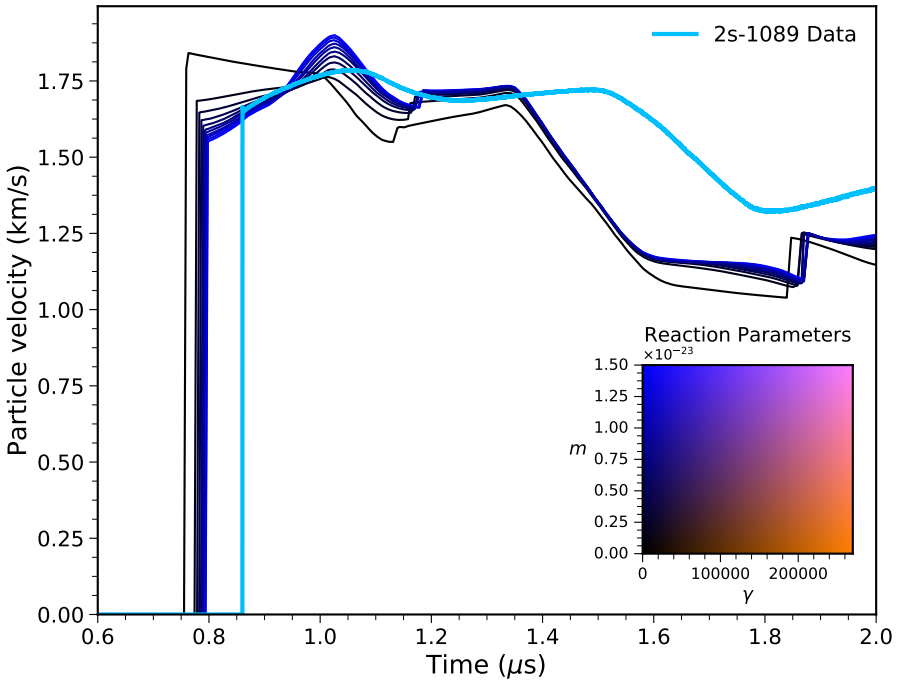

Figure 16: Simulation results using the SRFM rate equation when $\gamma = 1900$ for various values for the effective mass, m, being compared to shot 2s-1089. The Arrhenius parameters for these simulations are $Z = 430$ and $T_{\mathrm{a}} = 7760$.

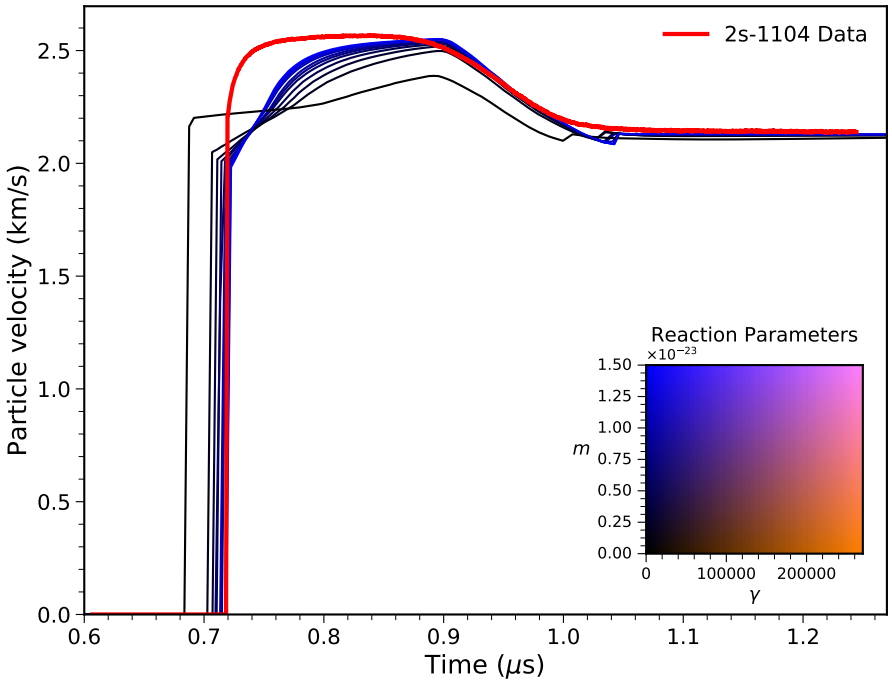

Figure 17: Simulation results using the SRFM rate equation when $\gamma = 1900$ for various values for the effective mass, m, being compared to shot 2s-1104. The Arrhenius parameters for these simulations are $Z = 430$ and $T_a = 7760$.

References

[1] R. C. Huber, J. H. Peterson, J. D. Coe, D. M. Dattelbaum, L. L. Gibson, R. L. Gustavsen, and S. A. Sheffield, "Polysulfone shock compressed above the decomposition threshold: Velocimetry and modeling of two-wave structures," *Journal of Applied Physics*, 2020. (in press).

[2] S. M. Valone, "An extension of transition-state theory for shock-induced chemical kinetics," *The Journal of Chemical Physics*, vol. 118, no. 14, pp. 6289–6297, 2003.

[3] C. E. Morris, J. N. Fritz, and R. G. McQueen, "The equation of state of polytetrafluoroethylene to 80 GPa," *The Journal of Chemical Physics*, vol. 80, no. 10, pp. 5203–5218, 1984.

[4] D. M. Dattelbaum, "In situ insights into shock-driven reactive flow," *AIP Conference Proceedings*, vol. 1979, no. 1, p. 020001, 2018.

[5] D. M. Dattelbaum, J. D. Coe, C. B. Kiyanda, R. L. Gustavsen, and B. M. Patterson, "Reactive, anomalous compression in shocked polyurethane foams," *Journal of Applied Physics*, vol. 115, no. 17, p. 174908, 2014.

[6] D. M. Dattelbaum, J. D. Coe, P. A. Rigg, R. J. Scharff, and J. T. Gammel, "Shockwave response of two carbon fiber-polymer composites to 50 gpa," *Journal of Applied Physics*, vol. 116, no. 19, p. 194308, 2014.

[7] A. Fredenburg, J. Coe, K. Maerzke, J. Lang, D. Dattelbaum, and D. Sandoval, "Estimating the reaction onset for porous polymer systems," *AIP Conference Proceedings*, vol. 1979, p. 090003, 2018.

[8] D. Lacina, C. Neel, and D. Dattelbaum, "Shock response of poly[methyl methacrylate] (PMMA) measured with embedded electromagnetic gauges," *Journal of Applied Physics*, vol. 123, no. 18, p. 185901, 2018.

[9] W. J. Carter and S. P. Marsh, "Hugoniot equation of state of polymers," Tech. Rep. LA-13006-MS, Los Alamos National Laboratory, 1995.

[10] D. J. Tannor and D. Kohen, "Derivation of kramers' formula for condensed phase reaction rates using the method of reactive flux," *The Journal of Chemical Physics*, vol. 100, no. 7, pp. 4932–4940, 1994.

[11] J. H. Peterson and J. D. Coe, "Hydrodynamic simulations of shock-driven chemistry in polyimide," *AIP Conference Proceedings*, 2019. (in press).

[12] R. Menikoff, "Arrhenius rate: constant volume burn," tech. rep., Los Alamos National Laboratory, 2017. LA-UR-17-31024.

[13] R. C. Huber. Personal Communication, 2019.